A LAGROBO Multiproperty Fit to Four-Atom Potential Energy Surfaces: The OH + HCl Case Study†

Ernesto Garcia and Aurelio Rodriguez

Departamento de Química Física, Universidad del País Vasco, 01006 Vitoria, Spain

M. Luz Hernández

Departamento de Física de la Atmósfera, Universidad de Salamanca, 37008 Salamanca, Spain

Antonio Laganà*

Dipartimento di Chimica, Università di Perugia, 06123 Perugia, Italy

Received: March 5, 2003; In Final Form: May 6, 2003

The four-atom LAGROBO functional form has been used to fit the ab initio potential energy values of the OH + HCl → C^+ + H_2O reaction. A multiproperty analysis of the fitted surfaces based on the value of the rate coefficients and on the fraction of energy disposed into product vibration has prompted the development of a more general and flexible functional. Using the improved LAGROBO functional, it has been possible to play with the height of the barrier and with the depth of the entrance channel well to significantly reduce the difference between calculated and measured properties of the OH (OD) + HCl reactions.

1. Introduction

Quantitative information on the efficiency of reactive systems and on the characteristics of their measured properties can be easily obtained by performing dynamical calculations in which the interaction is appropriately dealt (see for example refs 1−4). This is usually obtained by constructing a suitable potential energy surface (PES).

Useful guidelines for carrying out a proper fitting and/or interpolation of a PES starting from a sufficiently extended grid of ab initio points have been recently discussed in ref 5. In that paper, two main families of fitting and interpolation methods are described. The first family is that of global functional forms. Global methods expand the potential in terms of some particular basis functions valid over the whole range of definition of the considered variables and make use, for example, of a least-squares (LS) technique to approximate or reproduce the given electronic energy values. As an alternative to this, use can be made of piecewise spline and Morse-spline techniques utilizing basis functions that are non zero and polynomial-like over a finite range of grid points. Due to the increase of memory capacity of present computers the importance of the other family of methods (the local ones) has also increased. Accordingly, the Shepard interpolation techniques (in which the potential energy surface is represented by a weighed sum of Taylor expansions local to each given ab initio point) and the moving LS technique (that couples the global least-squares method with the use of basis functions local to the geometry of interest) are also becoming increasingly popular.

The validity of the fitted PES is usually evaluated by comparing observable properties calculated on it with available experimental data. This type of validation is based on the possibility of moulding the critical features of the PES to lead to a satisfactory reproduction of available measured quantities (multiproperty analysis). The modification of specific features of a PES is not an easy exercise because local methods may make it difficult to connect smoothly different zones of the interaction (especially long-range ones) whereas global ones may make it impossible to introduce corrections having a local effects and avoid incontrollable situations.

In this paper we discuss the fitting of the OH + HCl potential energy surface based on the use of bond order (BO) variable global approaches. In the paper various PESs are fitted and tested by carrying out a multiproperty analysis based on quasiclassical trajectory (QCT) estimates of the measured kinetic and spectroscopic properties of the system.

The paper is organized as follows: In section 2 some BO approaches to the fitting of ab initio potential energy values are illustrated. In section 3 the LAGROBO procedure is applied to the OH + HCl system. In section 4 a multiproperty test of the fitted PESs is performed and the need for improving the description of the fixed angle minimum energy paths (MEP) is discussed. In section 5 a new LAGROBO fitting procedure is developed and results obtained from it by performing QCT calculations are analyzed.

2. The Global BO Functional Forms

As already mentioned, in recent years, we have developed some approaches to the global fitting of few atom potential energy surfaces based on the use of BO coordinates. This is motivated by the fact that whereas the coordinates commonly used to formulate dynamical equations of few atom reactive systems are orthogonal and arrangement-like (most often Jacobi), the coordinates preferred for the formulation of the related interaction are of the non orthogonal type (though some examples of the use of nonorthogonal coordinates to formulate the atom diatom Hamiltonian are given in the literature[6−10]).

† Part of the special issue "Donald J. Kouri Festschrift".

10.1021/jp030304i CCC: $25.00
Published on Web 07/19/2003

Typically, in fact, the global formulations of the interaction for a system of N atoms are based on $N(N-1)/2$ internuclear distances (or a combination of internuclear distances and related angles), which are the most popular nonorthogonal coordinates.

2.1. BO Polynomials. Among the nonorthogonal coordinates the BO ones exhibit features of particular relevance to the functional representation of atomic and molecular interactions. The BO coordinate n_i for the i*th* pair of atoms is defined as

$$n_i = \exp[-\beta_i(r_i - r_i^\circ)] \tag{1}$$

where β_i and r_i° are empirical parameters. As apparent from the definition, BO coordinates tend to zero as the related internuclear distances tend to infinity and circumscribe the representation of the interaction inside a limited interval. This makes BO polynomials naturally converge at large distance with no need for artificial damping functions. As a matter of fact, BO polynomials have already been used to fit the potential energy of two-[11] and three-[12−18] atom systems.

The parameters of a BO polynomial potential can be determined from the spectroscopic properties of the related diatomic molecule.[19] Such a relationship takes an analytical form when the potential is modeled as a second-order BO polynomial (Morse potential). When the atom−atom interaction is modeled using a higher order polynomial, the parameters can be determined by optimizing the reproduction of the higher order diatomic force constants and/or long-range dispersion forces.[11] In this case the procedure is based on the numerical solution of a simple algebraic equation. In the case of atom diatom reactive systems, the two-body terms of the many body expansion of the interaction[20] are formulated as fourth-order polynomials in the related BO coordinate whereas the three-body term is given as a polynomial of the sixth order (made only of crossed terms).[12]

This approach is presently being extended to many atoms using a pseudo pair additive form of the type[9,10]

$$V(\{n\}) = \sum_i D_i(1 + Q_i(\{n_k\}_{k\neq i}))P_i(n_i) \tag{2}$$

where i runs over all diatomic pairs and Q_i and P_i are low-order polynomials. Q_i depends an all the BO variables but n_i. P_i depends directly only on n_i and parametrically also on the remaining n_k variables. Using a Wilson transformation,[21] BO representations can also be converted locally into a normal coordinate one for the geometries of interest. This makes the treatment more complex and may, in certain cases, introduce some numerical instabilities.

2.2. HYBO Functional Representations. A different way of tackling the problem is to describe the overall interaction in terms of contributions associated with specific percourses (channels) connecting a given arrangement (usually the reactant one) to another arrangement (for example that of a given specific product). Accordingly, each of these reaction channels can be described by a rotation of a BO (ROBO) pseudo diatomic-like model potential from an asymptotic form to another asymptotic form. Such a rotation is accompanied by the gradual transformation of the values of the parameters of the model from those of the reactants into those of the products involved. The reactive transformation follows the progress of a particular coordinate called reaction coordinate.

The model is formulated in hyperspherical BO (HYBO) coordinates which, for the collinear A + BC → AB + C reactive process, read as

$$\rho = \sqrt{{n_{AB}}^2 + {n_{BC}}^2}$$
$$\alpha = \arctan n_{BC}/n_{AB} \tag{3}$$

The angle α varies from 0 to $\pi/2$ when a pure reactant is transformed to a pure product oscillator. For this reason α is usually taken as the reaction coordinate of the reactive process. At each value of α the hyperradius ρ varies from zero (full dissociation) to $\sqrt{\exp[2\beta r_{BC}^\circ]+\exp[2\beta r_{AB}^\circ]}$ (complete collapse) acting as a bound coordinate describing the collective motion of the system that ensures the conversion of the internal energy of the reactants into that of the products.[22] A simple (Morse like) formulation of the ROBO potential in HYBO coordinates for the collinear reactive process P of the type A + BC → AB + C is where D^P is the depth of the channel and $\rho_\circ$ is the location of its minimum along ρ

$$V^P(\rho,\alpha) = D^P(\alpha)\left[\frac{\rho^2}{\rho_\circ^2(\alpha)} - 2\frac{\rho}{\rho_\circ(\alpha)}\right] \tag{4}$$

The reaction channel is then shaped by assuming a suitable functional dependence of D^P and $\rho_\circ$ on α.

2.3. LAGROBO Functional Representations. It is worth emphasizing here that, as already pointed out before (see also refs 22−24) ρ and α are process (nonorthogonal) coordinates. They can, in fact, properly describe only one ROBO and one particular collinear process P connecting a given asymptotic arrangement to another asymptotic arrangement (though they still cover the full configuration space). Additional HYBO coordinates and more than one ROBO potential are needed to describe more realistic reactive processes.

In the simplest realistic case, the full-dimensional A + BC atom diatom reaction, one needs the (additional) angle Φ (Φ is the angle formed by the two internuclear distances explicitly considered in the reactive process) and two additional ROBO terms (associated with the two other possible reactive processes). Accordingly, the ROBO terms have the general form

$$V^P(\rho,\alpha,\Phi) \equiv D^P(\alpha;\Phi)\, F^P(\rho;\alpha,\Phi) \tag{5}$$

where, strictly speaking, also the HYBO coordinates (and not only the functions) should be labeled after the process. $D^P(\alpha;\Phi)$ is a function of α describing the MEP of process P (parametrically depending on Φ). $F^P(\rho;\alpha,\Phi)$ is a function of ρ describing the shape of the reaction channel of process P (parametrically depending on Φ and α). The three ROBO terms need to be combined in a way that offers at each geometry of the system the most appropriate description of the interaction. This is obtained by taking a linear combination of the three ROBO terms and by weighing them proportionally to their closeness to collinearity (from this the name LAGROBO that means Largest Angle Generalization of the ROBO).

The LAGROBO functional form has been successfully used to fit the potential energy surface of some three-atom systems.[23,24] Recently it has also been extended to formulate the interaction of four-atom systems[25] and applied to the multiproperty analysis of the PES of OH + H_2[26−28] and OH + HCl.[29] Also when going from three- to four-atom systems, one needs to define more angles and add other ROBO contributions. The way the bonds and the angles are defined may vary. This impacts not only the type and the numbers of ROBO terms significantly contributing to the assemblage of the LAGROBO functional but also the possibility of connecting smoothly the various regions of the PES.

3. Data and LAGROBO Procedure for OH + HCl

As already mentioned, the general formulation of the LAGROBO PES is given by a combination of the ROBO functionals V^P of all the reaction channels

$$V = \frac{\sum_P w^P V^P}{\sum_P w^P} \tag{6}$$

contributing to the reactive process weighed by the coefficient w^P related to the closeness of the considered geometry to the collinear one. For the OH + HCl system, the reaction channels considered can be found in ref 45 and the weighting function used can be found in ref 25.

3.1. Four-Atom LAGROBO Functional. In the case of four-atom systems the sum of eq 6 includes, in principle, 12 contributing V^P terms. In this case the V^P terms have the form[25]

$$V^P = D^P F^P + I^P \tag{7}$$

where the product $D^P F^P$, as already seen, is the ROBO-like model potential of process P, and I^P is a corrective term due to the effect of the remaining atom−atom pair (in the case of four-atom systems it is one term only). The ROBO terms ensure the correct reproduction of both the asymptotic properties and the characteristics of the fixed collision angle MEPs derived from the ab initio data (eventually modified to incorporate corrective experimental information). For three atom systems they are given the simple quadratic form

$$D^P F^P \equiv D(\alpha,\sigma;\tau,\delta,\gamma)\left[\frac{\rho^2}{\rho_o{}^2(\alpha,\sigma;\tau,\delta,\gamma)} - \frac{2\rho}{\rho_o(\alpha,\sigma;\tau,\delta,\gamma)}\right] \tag{8}$$

To shape the fixed angle MEPs, the parameters of the different V^P ROBO terms (the location of the reaction channel energy minimum, $\rho_o(\alpha,\sigma;\tau,\delta,\gamma)$, and of its depth, $D(\alpha,\sigma;\tau,\delta,\gamma)$, are given as functions of the angles α and σ parametrically dependent on the other angles τ, δ, and γ.

For the generic tetratomic system κ, λ, μ, and ν, the α and σ angles are defined as

$$\alpha = \arctan\left(\frac{n_{\mu\nu}}{n_{\kappa\lambda}}\right) \qquad \sigma = \arccos\left(\frac{n_{\lambda\mu}}{\rho}\right)$$
$$\rho = \sqrt{n_{\kappa\lambda}{}^2 + n_{\lambda\mu}{}^2 + n_{\mu\nu}{}^2} \tag{9}$$

($n_{\eta\xi}$ is the BO coordinate of the $\eta\xi$ pair of atoms) whereas the angles τ, δ, and γ are defined as

$$\tau = \sqrt{\phi'^2 + \psi'^2 + \theta'^2} \qquad \delta = \arctan\left(\frac{\psi'}{\theta'}\right)$$
$$\gamma = \arccos\left(\frac{\phi'}{\tau}\right) \tag{10}$$

(see ref 25) with

$$\phi' = 2\pi - 2\phi \qquad \psi' = 2\psi - 2\pi \qquad \theta' = 4\theta \tag{11}$$

The physical angles ϕ, ψ, and θ defining the geometry and the relative orientation of the tetratomic system are shown in Figure 1. The term I^P concerned with the interaction of the diatom $\kappa\nu$ with the diatomic pair $\lambda\mu$ is expressed as

$$I^P \equiv I^P(n_{\kappa\nu};\bar{n}) = D_{\kappa\nu} S(\bar{n})(n_{\kappa\nu}{}^2 - 2n_{\kappa\nu}) \tag{12}$$

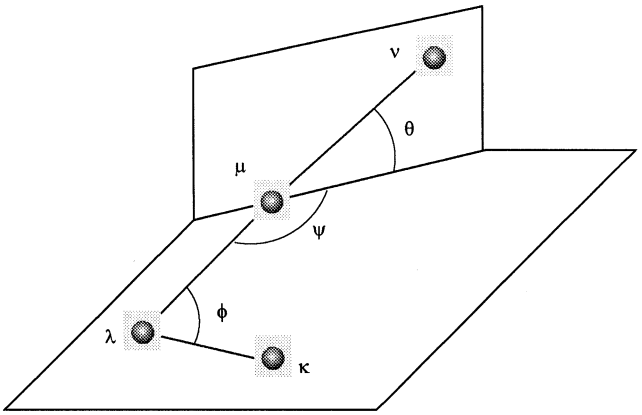

Figure 1. Sketch of the angular variable definition of ref. [25].

with $\bar{n} = (n_{\kappa\lambda} + n_{\mu\nu})/2$, $D_{\kappa\nu}$ being the dissociation energy of the $\kappa\nu$ diatom and $S(\bar{n})$ being a switching function equal to $1 + \cos[\pi(\bar{n} + p)/2p]$ for $\bar{n} < p$ and zero elsewhere.

3.2. Fitting Procedure. To determine the value of the surface parameters (see ref 29), the fixed τ, δ, and γ minimum energy paths of the $\alpha\sigma$ planes were first drawn using the ab initio potential energy values. Then, the values of $\rho_o(\alpha,\sigma;\tau,\delta,\gamma)$ and $D(\alpha,\sigma;\tau,\delta,\gamma)$ at the asymptotes and at the saddle to reaction were interpolated using a trigonometric (square cosine) function (having a maximum at the interval midpoint and vanishing at the extrema) multiplied by an additional factor enforcing the reproduction of the slope of the related MEP. This ensured that all the fixed τ, δ, and γ MEPs could reproduce not only the asymptotes but also the location and the height of the related barrier to reaction. The variation of ρ_o and D at the saddle to reaction, TS, ($\rho_{oTS}(\tau;\delta,\gamma)$ and $D_{TS}(\tau;\delta,\gamma)$, respectively) with the angles τ, δ, and γ (that is, as a function of the relative orientation of the system) was determined by singling out first their dependence on the value of the angle τ (the value of τ is a measure of the collinearity of the system). The same approach was adopted for $\alpha_{TS}(\tau;\delta,\gamma)$ and $\sigma_{TS}(\tau;\delta,\gamma)$ (the value of α and σ at the TS).

The dependence of $\rho_{oTS}(\tau;\delta,\gamma)$, $D_{TS}(\tau;\delta,\gamma)$, $\alpha_{TS}(\tau;\delta,\gamma)$, and $\sigma_{TS}(\tau;\delta,\gamma)$ on τ was determined by calculating their values at $\tau = 0$, $\tau = \tau_1 > 0$, and $\tau = \tau_2 > \tau_1$ and using a second-order polynomial to cover the whole interval. The dependence of these functions on γ and δ was formulated in terms of a Fourier series in γ whose coefficients are polynomials in δ. As an example, D_{TS} at $\tau = \tau_1$ reads

$$D_{TS,\tau_1}(\gamma;\delta) = \frac{c_o(\delta)}{2} + \sum_{l=2,4,6,8} [c_{l-1}(\delta)\sin(l\gamma) + c_l(\delta)\cos(l\gamma)] \tag{13}$$

where the c coefficients are further expressed as

$$c_i(\delta) = \sum_{j=0}^{6} c_{ij}\delta^j \tag{14}$$

Among the c_{ij} coefficients a key role is played by c_{00} because it determines the height of the barrier to reaction. The same procedure was adopted for $\rho_{oTS,\tau_1}(\delta,\gamma)$, $\sigma_{TS,\tau_1}(\delta,\gamma)$, and $\alpha_{TS,\tau_1}(\delta,\gamma)$ and at $\tau = \tau_2$ for $D_{TS,\tau_2}(\gamma,\delta)$, $\rho_{oTS,\tau_2}(\gamma,\delta)$, $\sigma_{TS,\tau_2}(\delta,\gamma)$, and $\alpha_{TS,\tau_2}(\delta,\gamma)$.

3.3. Theoretical and Experimental Data. Ab initio information on the OH + HCl reaction was obtained by Clary, Nyman, and Hernandez (CNH) who developed a potential energy surface (PES)[30] by combining a LEPS functional describing the interac-

tion of the O + HCl → OH + Cl process with the Carter−Murrell functional for the water molecule of ref 31. On the CNH PES, theoretical rate coefficients were calculated using a reduced dimensionality RBA quantum approach.[32] Later on, Steckler and co-workers (STWB) determined the minimum energy path (MEP) by evaluating the most favored geometries of the system using an MBPT(2)/DZP method and the related energies using a CCSD(T)/PVQZ method.[33] These data will be considered as the reference ab initio values throughout this paper. On the PES built around these data, rate coefficients of the OH + HCl reaction were calculated using a transition state (TS) theory approach.[33,34] Recently, Yu and Nyman (YN) carried out further RBA dynamical calculations on a PES based on the interpolation of new ab initio potential energy values computed using a UMP2 technique and a scaling correction.[35] To fit the CNH and YN surfaces, the saddle energy was lowered significantly from its original ab initio value to reproduce the experimental rate coefficients.

Measured data of the global reactive OH + HCl process with which to compare theoretical outcomes are provided by some kinetic experiments that produced a set of thermal reaction rate coefficients $k(T)$. Most of the measurements were performed in the years 1984−85 for values of the temperature T ranging from 200 to 1000 K. Measured rate coefficients were fitted using empirical expressions.[36−39] More recently, Smith and collaborators measured the rate coefficients at lower temperature (138−298 K)[40] whereas Ravishankara and collaborators repeated their experiment for T values ranging from 200 to 400 K.[34] It is worth noting here that measured rate coefficients are almost independent of temperature for values of T smaller than 298 K. On the contrary, for values of T larger than 298 K an increase of the rate coefficient with temperature is observed. The temperature dependence of $k(T)$, recommended by IUPAC[41] for the experimental range of T, is given by the three-parameter curve $k(T) = 3.28 \times 10^{-17} T^{1.66} \exp[184/T]$ cm^3 molecule^{-1} s^{-1}, proposed by Ravishankara and collaborators.[34] We shall use these values throughout the paper to compare calculated values of the rate coefficient with the experiment even if the curve slightly underestimates the IUPAC recommended value at $T =$ 298 K (8.0×10^{-13} cm^3 molecule^{-1} s^{-1}) and the measurements performed by Smith at low temperature.

Another kind of experimental information with which to match the calculated properties of the OH + HCl reaction was obtained by Setser and Butkovskaya.[42] They measured the room-temperature vibrational spectrum for the H_2O and DOH molecules produced in the OH + HCl reaction and its OD + HCl isotopic variant. No appreciable infrared chemiluminescence was measured for the OH + HCl reaction whereas the measured intensity of emission for the OD + HCl reaction was large. This was rationalized by assuming that, in the OH case, the vibrational energy of the product water molecule is mainly disposed into the bending mode that deexcites by collision with the HCl molecules of the bulk, whereas the OD reaction preferentially allocates vibrational energy into the stretching modes of the product molecule that does not deexcite by collision with the bulk HCl.

3.4. LGR*x* PESs. Thanks to the flexibility of the LAGROBO functional, we created three LAGROBO PESs[29] called LGR*x* (with *x* being a sequential number) that naturally match not only the asymptotic properties of the system (as from spectroscopic data[19,43]) but also the geometry of the system at the saddle to reaction (ab initio values taken from refs 33 and 35 were used for the fit). Ab initio values were empirically modified so as to generate three LAGROBO PESs (LGR1, LGR2, and LGR3) differing almost exclusively for the height of the saddle to reaction and the associated imaginary frequency (see Table 1 where the properties of LGR2 are compared with those of LGR3).

TABLE 1: Properties of the Molecular Geometry at the Saddle to Reaction of the Various Surfaces for the OH + HCl System[a]

	CNH	STWB	YN	LGR2	LGR3	LGR2W	LGR3W	LGR1N	LGR6N
energy	0.24	2.43	2.06	0.55	1.00	0.55	1.00	2.43	1.80
r_{HO}	0.978	0.98	0.968	0.981	0.981	0.955	0.956	0.979	0.979
r_{OH}	1.169	1.31	1.258	1.293	1.280	1.242	1.242	1.315	1.315
r_{HCl}	1.429	1.40	1.405	1.429	1.426	1.404	1.404	1.397	1.397
ϕ	110	104	104	103	103	104	104	102	102
ϵ	167	143	142	150	150	150	150	144	144
ζ	180	59	52	56	56	58	57	54	55
ω_1	394	395	344	549	456	384	381	358	360
ω_2	590	511	566	686	658	680	678	590	600
ω_3	597	858	931	956	939	956	953	1214	1219
ω_4	1669	1388	1400	1419	1402	1486	1478	1499	1512
ω_5	3603	3695	3846	3837	3813	3765	3758	3493	3491
ω_i	1370	1413	2023	382	707	1772	1918	1413	1413

[a] Distances are given in ångstroms, angles in degrees, frequencies in cm^{-1}, and energies in kcal mol^{-1}.

In particular, the ab initio value of the saddle to reaction (2.43 kcal mol^{-1}) was lowered to 2.28, 0.55, and 1.00 kcal mol^{-1} for LGR1, LGR2, and LGR3, respectively. As for the frequencies, for example, the LGR3 values of the small ones (ω_1, ω_2, and ω_3) disagree by a few tens of cm^{-1} (a fairly acceptable error in absolute terms although percentually quite large) and are systematically higher than the ab initio ones. Also the large frequencies (ω_4 and ω_5) differ by some tens of cm^{-1}. In this case, however, the maximum deviation is only 2% with respect to the most accurate ab initio value for ω_4 and 4% for ω_5 (the two sets of ab initio values show a similar difference[33,35]). The most important deviation occurs for the imaginary frequency ω_i. The LGR3 imaginary frequency is 50% the ab initio value[33] (the imaginary frequency of the other ab initio[35] calculation is 40% higher). As expected, Table 1 shows also that the length of the OH bonds, the angle formed between them, the length of the HCl bond, the HO−H−Cl angle, and the torsion angle of LGR3 are not only similar to the ab initio data but they are also quite close to the values associated with the other LAGROBO surfaces (after all, the two sets of ab initio data show differences of the same type).

4. Descriptor of the Fixed Angle MEPs

A key feature of the LGR*x* PESs is the square cosine formulation of the descriptor of the fixed angle MEPs and its calibration on the height of the saddle to reaction. To investigate the effect of this choice on the performance of the PES, we carried out a multiproperty analysis of the LGRx surfaces.

4.1. Multiproperty Test of LGR*x* PESs. On the LGR*x* surfaces we first calculated, using quasiclassical trajectories, the rate coefficients for a set of temperatures spanning the range covered by the experiments (138−1055 K). Details of the QCT calculation are given in ref 29. The rate coefficients calculated on the LGR3 PES well reproduce the measured temperature dependence and led to a root-mean-square percentual deviation from the experimental data as low as 22%.[29] On the contrary, the rate coefficients calculated on LGR1 and LGR2 largely underestimate and overestimate, respectively, the measured value. For the same reason, the subsequent step of the multiproperty analysis was carried out only for LGR3.

When the analysis was extended to the energy disposed into product vibration at $T = 298$ K for both the OH + HCl and

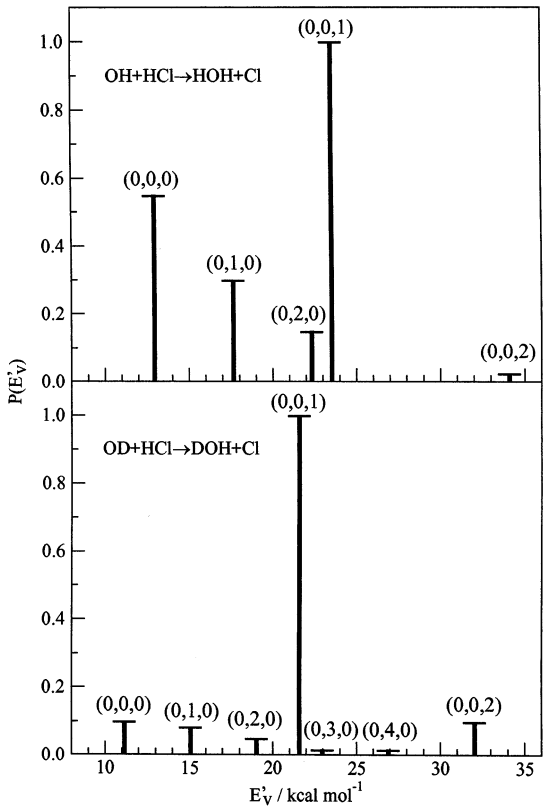

Figure 2. Vibrational distribution of the H_2O product (upper panel) and of the DOH product (lower panel) calculated on the LGR3 PES at $T = 298$ K. The notation (v_{str1}, v_{bend}, v_{str2}) indicates the quantum numbers for the stretching of the old OH bond, the bending of the HOH or DOH angle, and the stretching of the new OH or OD bond, respectively. Only single bending and new OH or OD bond stretching excitations are shown.

OD + HCl reactions (see Figure 2 where the excitation of the bending and of the stretching modes calculated on LGR3 are shown only for the new OH or OD bonds), theoretical results were in clear disagreement with the experiment. They showed, in fact, that on the LGR3 PES the system reacts by mainly exciting the stretching mode of the product molecule for both isotopes, contrary to the conclusions of ref 42. This inability of the dynamical calculations performed on the LGR*x* PES to match the information provided by the infrared emission spectroscopy experiment prompted the question of what is the feature mainly responsible for the unsatisfactory allocation of the energy into product modes.

A detailed inspection of the LGR3 PES showed that, indeed, a square cosine function is not flexible enough to satisfactorily describe the slope of the fixed angle MEPs. In particular, it cannot take a value lower than zero. This suggested to modify the LAGROBO fitting procedure so as to fit in a more realistic way the structure of the PES along the minimum energy path and, in particular, as is the case of the OH + HCl system, the entrance channel well.

4.2. Incorporation of the Entrance Channel Well. A first attempt to reproduce the entrance channel well into the LAGROBO fitting procedure was carried out by adding the extra term $D_{vdw}(\tau,\delta,\gamma)$ to the function shaping the MEPs of the fixed δ, γ, and τ angle $\alpha\sigma$ plane.

For illustrative purposes, the saddle and the well minimum points as well as the reactant and the product asymptotes of the MEP of the $\kappa\lambda + \mu\nu \rightarrow \kappa\lambda\mu + \nu$ reaction channel are marked in Figure 3 as crosses. On every $\alpha\sigma$ plane the location of the asymptotes is fixed;[25] the $\kappa\lambda + \mu + \nu$ and $\kappa\lambda + \mu + \nu$ atom−

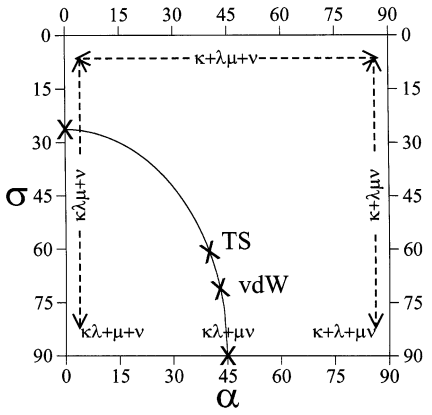

Figure 3. Geometrical properties of the minimum energy path for the $\kappa\lambda + \mu\nu \rightarrow \kappa\lambda\mu + \nu$ process in the $\alpha\sigma$ plane at a given orientation of the atoms of the system. Crosses indicate the stationary points. Angles are given in degrees.

atom−diatom configurations are located at ($\alpha = 0°$, $\sigma = 90°$) and ($\alpha = 90°$, $\sigma = 90°$), respectively, the $\kappa + \lambda\mu + \nu$ atom−atom−diatom configuration is located at the $\sigma = 0°$ line, the $\kappa\lambda + \mu\nu$ diatom−diatom configuration is located at the point ($\alpha = 45°$, $\sigma = 90°$), and the $\kappa\lambda\mu + \nu$ and $\kappa + \lambda\mu\nu$ atom−triatom configurations are located at the $\alpha = 0°$ and $\alpha = 90°$ lines, respectively. Then, to shape the (fixed δ, γ, and τ) MEPs the various portions of the $D(\alpha,\sigma;\tau,\delta,\gamma)$ function (i.e., from the reactants to the well, from the well to the saddle, and from the saddle to the products) were fitted separately using low-order polynomials.

The coefficients of these polynomials are straightforwardly determined from the values of the energy at the stationary points (including the asymptotes) and the related derivatives to ensure the continuity. The formulation of the asymptotic OH, HCl, and H_2O potentials is again the same as for the previous LAGROBO surfaces.

The same functions used in LGR3 were adopted to formulate $D_{TS}(\tau,\delta,\gamma)$ (the energy at the saddle to reaction on the $\alpha\sigma$ plane at fixed τ,δ,γ values) as well as the asymptotic OH, HCl, and H_2O potentials. The function used to formulate $D_{vdw}(\tau,\delta,\gamma)$ (the depth of the entrance channel well on the $\alpha\sigma$ plane at fixed τ, δ, γ values) is a Gaussian function

$$D_{vdw}(\tau,\delta,\gamma) = p_o \exp[-p_1(p_2(\theta - \theta_{vdw})^2 + p_3(\psi - \psi_{vdw})^2 + p_4(\varphi - \varphi_{vdw})^2 + p_5(n_{OH} - n_{OHvdw})^2 + p_6(n_{HCl} - n_{HClvdw})^2)] \quad (15)$$

in which the dependence on τ, δ, and γ is formulated via that on θ, ψ, and φ (see eqs 10 and 11). Note the dependence on the BO coordinates n_{HCl} of the new HO bond and the old HCl bond, respectively, rather than in the HYBO ones. The Gaussian function is centered at the minimum of the entrance channel well[35] ($\theta_{vdw} = 0°$, $\psi_{vdw} = 173.5°$, $\varphi_{vdw} = 112.8°$, $n_{OHvdw} = 0.0933$, and $n_{HClvdw} = 0.98066$) and has a depth $p°$ of −5.46 kcal mol^{-1}. The set of values of the p coefficients optimizing the reproduction of the frequencies of the van der Waals complex[35] are $p_1 = 0.91$, $p_2 = 1.05$, $p_3 = 0.07$, $p_4 = 0.50$, $p_5 = 2.20$, and $p_6 = 0.80$.

4.3. Characteristics of the LGR*x*W PESs. Using the new type of LAGROBO functional enforcing the reproduction of the entrance channel well, two new PESs (LGR2W) and (LGR3W) were produced for the OH + HCl reaction. The first one (LGR2W) has a saddle to reaction of 0.55 kcal mol^{-1} (like the LGR2 surface) and the second one (LGR3W) has a height

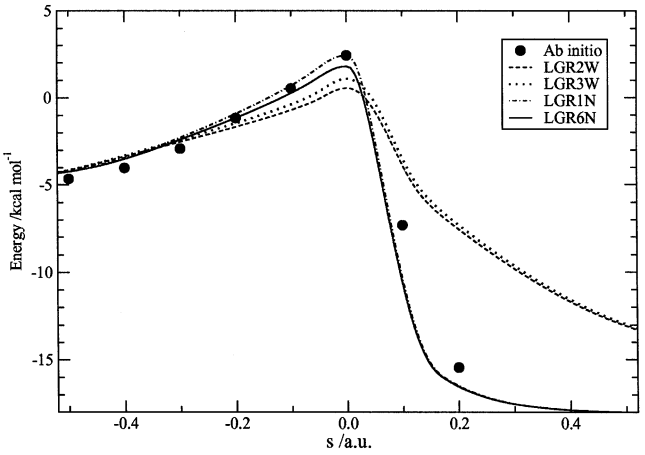

Figure 4. Minimum energy path for the various PESs: (solid circles) ab initio values; (dashed line) LGR2W; (dotted line) LGR3W); (dashed dotted line) LGR1N; (solid line) LGR6N.

TABLE 2: Properties of the van der Waals Minimum of the Various Surfaces for the OH + HCl Reaction[a]

	CNH	YN	LGR2W	LGR3W	LGR1N	LGR6N
energy	−2.13	−5.46	−5.45	−5.45	−5.45	−5.45
r_{HO}	0.981	0.968	0.968	0.968	0.972	0.972
r_{OH}	1.704	2.003	2.002	2.002	1.998	1.998
r_{HCl}	1.286	1.285	1.285	1.285	1.280	1.280
ϕ	104	113	114	114	114	114
ϵ	166	174	177	177	175	175
ζ	0	0	0	0	0	0
ω_1	112	135	103	104	121	121
ω_2	264	130	131	132	198	193
ω_3	272	331	328	329	344	345
ω_4	1260	450	452	453	457	458
ω_5	2813	2898	2897	2901	3037	3019
ω_6	3537	3838	3955	3955	3945	3945

[a] Distances are given in ångstroms, angles in degrees, frequencies in cm^{-1}, and energies in kcal mol^{-1}.

of the saddle to reaction of 1.00 kcal mol^{-1} (like the LGR3 surface). The properties of the saddle to reaction of LGR2W and LGR3W are compared with those of the other PESs in Table 1. The geometries of the TSs of the two surfaces are practically identical and do not differ significantly from that of LGR2, LGR3, and the ab initio values. Real frequencies of the system at the saddle to reaction of LGR2W and LGR3W do not show significant deviations from those of the ab initio values (like those of the LGR2 and LGR3 surfaces). On the contrary, the imaginary frequencies of LGR2W and LGRW3 are significantly higher than those of LGR2 and LGR3. This confirms that the insertion of the van der Waals well definitely changes the slope of the MEP and the related thickness of the barrier in the saddle region. This is clearly illustrated in Figure 4 where some of the relevant MEPs are plotted. These MEPs were calculated using the POLYRATE package with the Page−McIver integrator.[44] Please notice that the origin of the reaction coordinate is set at the saddle to reaction for all the surfaces (obviously, this does not imply that the system at the saddle of the various MEPs has the same geometry).

The characteristics of the well of LGR2W and LGR3W are given in Table 2 where they are also compared with those of the other surfaces. As is apparent from the table, the characteristics of the well of the LGR2W and LGR3W surfaces are almost coincident and well reproduce the depth of the well and the related geometry of the ab initio data[35] (this further confirms the fact that the LAGROBO functional is highly flexible and the modifications are of local nature). Deviations from the ab initio values of the related frequencies do not exceed a few percent for all but the smallest one.

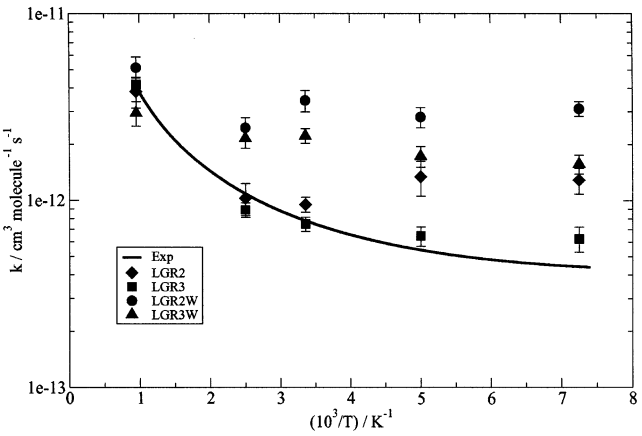

Figure 5. Rate coefficients plotted as a function of the inverse temperature: (solid line) recommended experimental results; (diamonds) LGR2; (squares) LGR3; (circles) LGR2W; (triangles) LGR3W.

4.4. Dynamical Properties. Extensive trajectory calculations were performed also on the LGR2W and LGR3W surfaces. The rate coefficients calculated on the LGR3W PES are smaller than those calculated on the LGR2W PES (see Figure 5) in agreement with the fact that the LGR3W saddle to reaction is higher than that of LGR2W. As apparent from Figure 5, the rate coefficients calculated on LGR2W and LGR3W are larger than any other (theoretical or experimental) estimate. This is in line with the expectation that by placing a well inside the entrance channel several large impact parameter trajectories, otherwise passing by as nonreactive, are driven into the interaction region where they can react. As a matter of fact, the maximum value of the impact parameter allowing reaction at $T = 298$ K that is 2.9 Å on LGR3 becomes 3.4 Å on LGR3W. This clearly implies that the lowering of the barrier (with respect to the original ab initio value) aimed at enhancing reactivity needs not be so drastic when the van der Waals well is included in the PES. This also confirms that the control of the reactive properties through the proposed variation of the LAGROBO functional is simpler than with most of the available functional representations of the interaction of polyatomic reactive systems.

Finally, it is important to emphasize here that the introduction of the well produced the expected effect of altering the structure of the product vibrational distribution.

5. Improved LAGROBO PESs

The above-mentioned advantages resulting from the incorporation of a well into the entrance channel of the LAGROBO PES motivated further work on building more general purpose (less ad hoc) flexibility into the related functional. This has led to a complete redesign of the descriptor of the fixed angle MEPs with the aim of reconducting the control of the stationary points of the surface under a scheme easier to generalize to polyatomic systems. In addition, a revision of the definition of the angular variables has been carried out to eliminate possible discontinuities at the edges of the interval of definition. For example, for coplanar configurations ($\theta = \theta' = 0$), like that at the saddle to reaction of the OH + H_2 reaction,[25] a discontinuity arises at $\psi = \pi$ for δ. In this case, in fact, for $\psi > \pi$ ($\psi' > 0$), δ is always $\pi/2$ whereas for $\psi < \pi$ ($\psi' < 0$) δ is always $-\pi/2$.

5.1. LAGROBO Functional. In the new formulation of the LAGROBO functional the angular coordinates are redefined. In particular, although ϕ is still the angle formed by the $\kappa-\lambda$

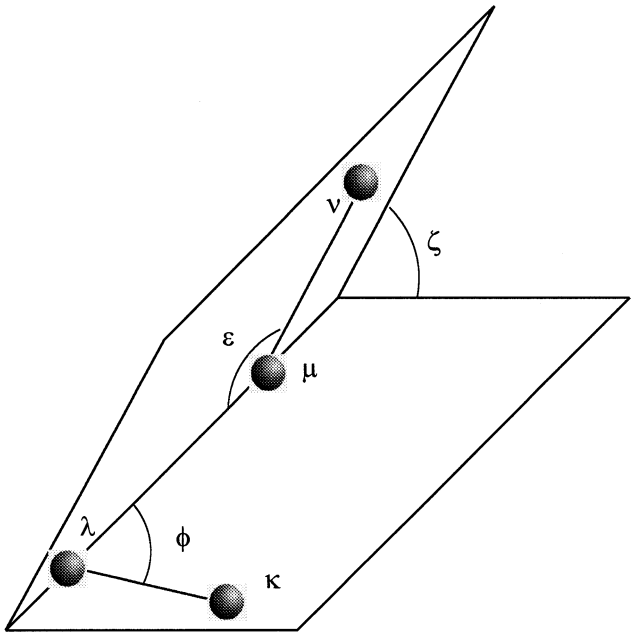

Figure 6. Sketch of the new angular variable definition.

and $\lambda-\mu$ bonds (as in the old formulation), ϵ and ζ (see Figure 6) are defined as ϵ is the angle formed by the $\lambda-\mu$ and $\mu-\nu$ bonds and ζ is the dihedral angle formed by the $\kappa\lambda\mu$ and $\lambda\mu\nu$ planes.

The second novelty of the new LAGROBO functional is the different formulation of the dependence of ρ_{oTS}, σ_{TS}, and α_{TS} on the internal angular coordinates. As already mentioned in section 2, in the previous formulation the values of ρ_{oTS}, σ_{TS}, and α_{TS} were calculated at the collinear ($\tau_0 = 0$) geometry, at the saddle to reaction ($\tau_1 = \tau_{TS}$) and at a third configuration ($\tau_2 > \tau_{TS}$). At each of these three values of τ (τ_0, τ_1, and τ_2), D_{TS}, ρ_{oTS}, σ_{TS}, and α_{TS} were expressed as a Fourier series in γ (eq 13) whose coefficients were then formulated as polynomials in δ (eq 14) and fitted using second-order polynomials in τ. In the new formulation the dependence of D_{TS}, ρ_{oTS}, σ_{TS}, and α_{TS} on ϕ, ϵ, and ζ is given explicitly by the relationships

$$D_{TS}(\phi,\epsilon,\zeta) = d_o + (d_1(\epsilon - \epsilon_{TS})^2 + d_2(\epsilon - \epsilon_{TS})^3 + (d_3 + d_4\epsilon^2)(\phi - d_5 - d_6\epsilon^2)^2) \times \exp[d_7(\epsilon - \pi)(\zeta - d_8 \exp(d_9(\epsilon - \epsilon_{TS})^2)]$$

$$\rho_{oTS}(\phi,\epsilon,\zeta) = (r_1 + r_2 \exp[r_3(\epsilon - \pi)^2](\phi - \phi_{TS})^3) \times (1 + r_4(\epsilon - \pi)(\zeta - \zeta_{TS})^2 + r_5(\epsilon - \pi)(\zeta - \zeta_{TS})^3)$$

$$\alpha_{TS}(\phi,\epsilon,\zeta) = ((a_1 + a_2(\epsilon - \epsilon_{TS}))(\phi - \phi_{TS}) + (a_3 + a_4(\epsilon - \epsilon_{TS}))(\phi - \phi_{TS})^2 + (a_5 + a_6(\epsilon - \epsilon_{TS}))(\phi - \phi_{TS})^3) \times \exp[a_7(\epsilon - \pi)(\zeta - \zeta_{TS})^2]$$

$$\sigma_{TS}(\phi,\epsilon,\zeta) = (s_1 + s_2(\epsilon - \epsilon_{TS}) + s_3(\phi - \phi_{TS})^2) \times \exp[s_4(\epsilon - \pi)(\zeta - \zeta_{TS})^2] \quad (16)$$

where ϕ_{TS}, ϵ_{TS}, and ζ_{TS} are the values of ϕ, ϵ, and ζ at the saddle to reaction TS[33] and the parameter d_o represents the height of the saddle of the global reaction. Please, notice the different meaning of the TS subindices in D_{TS}, ρ_{oTS}, σ_{TS}, and α_{TS} and in ϕ_{TS}, ϵ_{TS}, and ζ_{TS}. In the first case the subindex means the MEP barrier at fixed relative orientation of the system whereas in the second case it means the MEP barrier at the saddle for the overall reaction. The angles corresponding to the saddle are[33] $\phi_{TS} = 103.77°$, $\epsilon_{TS} = 143.42°$, and $\zeta_{TS} = 58.77°$. As is apparent from the above equations the analytical functions used for the new formulation of the LAGROBO PESs are extremely simple. The coefficients of these functions are optimized to reproduce the expected dependence of D_{TS}, ρ_{oTS}, σ_{TS}, and α_{TS} on the relative orientation of the system.

The procedure used for the introduction of the van der Waals well consists, as in the LGR*x*W PESs, in locating a new stationary point in the fixed angle MEPs. Then separate fittings for the various portions of the MEP connecting the reactants, the van der Waals well, the saddle to reaction, and the asymptotes are performed.

5.2. Further Improvements. To further increase the flexibility of the LAGROBO functional form, three other modifications were introduced. The first modification is concerned with the function used to model the depth of the van der Waals well on the MEP of the considered $\alpha\sigma$ planes. In the new LAGROBO functional the related Gaussian function (eq 15) is expressed in terms of the internuclear distances rather than in terms of the BO ones. Accordingly, $D_{vdw}(\tau,\delta,\gamma)$ is formulated as

$$D_{vdw}(\tau,\delta,\gamma) = p_o \exp[-p_1(p_2(\theta - \theta_{vdw})^2 + p_3(\psi - \psi_{vdw})^2 + p_4(\varphi - \varphi_{vdw})^2 + p_7(r_{HO} - r_{HOvdw})^2 + p_8(r_{OH} - r_{OHvdw})^2 + p_9(r_{HCl} - r_{HClvdw})^2)] \quad (17)$$

The angles and the distances corresponding to the minimum of the van der Waals well[35] are $\theta_{vdw} = 0°$, $\psi_{vdw} = 173.5°$, $\varphi_{vdw} = 112.8°$, $r_{HOvdw} = 0.9682$ Å, $r_{OHvdw} = 2.007$ Å, and $r_{HClvdw} = 1.285$ Å and p_o is its depth. The values of the p parameters are optimized to reproduce the frequencies of the van der Waals complex. Another change introduced in the new LAGROBO functional is the modification of the formulation of $D(\alpha,\sigma;\tau,\delta,\gamma)$ at the MEPs of the $\alpha\sigma$ planes from the saddle to the product asymptotes. To better reproduce the sharp decrease of the ab initio MEP[33] (see Figure 4), a two-term polynomial containing the sixth and the seventh power of the variable was used. Finally, a fourth-order polynomial (i.e., that as an additional parameter) was adopted to shape the portion of the MEP going from the van der Waals well to the saddle to better reproduce the ab initio value of the imaginary frequency of the associated arrangement.

5.3. New LGR*x*N PESs. Using the new formulation we have constructed a series of LAGROBO surfaces (named LGR*x*N where *x* is a sequential number) by empirically varying both the height of the barrier and the depth of the well. This is a simple task because one has to modify only the parameters d_o and p_o of eqs 16 and 17 and adjust the imaginary frequency at the saddle point by varying the coefficients of the previously mentioned fourth-order polynomial. All the other parameters are identical in the series of LGR*x*N PESs. Related values for the parameters of eq 16 are given in Table 3. The optimized parameters of eq 17 are slightly different from those obtained for the LGR3W surface: $p_1 = 0.90$, $p_2 = 1.05$, $p_3 = 0.09$, $p_4 = 0.60$, $p_7 = 0.10$, $p_8 = 0.10$, $p_9 = 0.10$.

The first of these new LAGROBO PESs (LGR1N), as illustrated in Figure 4, is fitted to the original unmodified ab initio values of both the barrier to reaction[33] and the van der Waals well,[35] i.e., $d_o = 2.43$ and $p_o = -5.46$ kcal mol^{-1}. The properties of the system at the saddle to reaction of the LGR1N surface are given in Table 1. In particular, both the bond lengths and angles obtained from ab initio calculations are well reproduced by LGR1N. The reproduction of the ab initio real

TABLE 3: Coefficients of the LGR*x*N PESs for $D_{TS}(\phi,\epsilon,\zeta)$, $\rho_{oTS}(\phi,\epsilon,\zeta)$, $\sigma_{TS}(\phi,\epsilon,\zeta)$, and $\alpha_{TS}(\phi,\epsilon,\zeta)$ (see Eq 16)

i	d_i	r_i	a_i	s_i
1	18.6821	1.3375	0.6809	1.2215
2	−13.1054	0.0295	0.0437	−0.0107
3	30.4364	−7.3531	−0.0827	−0.0671
4	−2.2236	0.0273	−0.1356	−0.0039
5	2.3504	0.0070	0.0089	
6	−0.0861		0.0146	
7	0.0262		0.0208	
8	1.2217			
9	−0.4290			

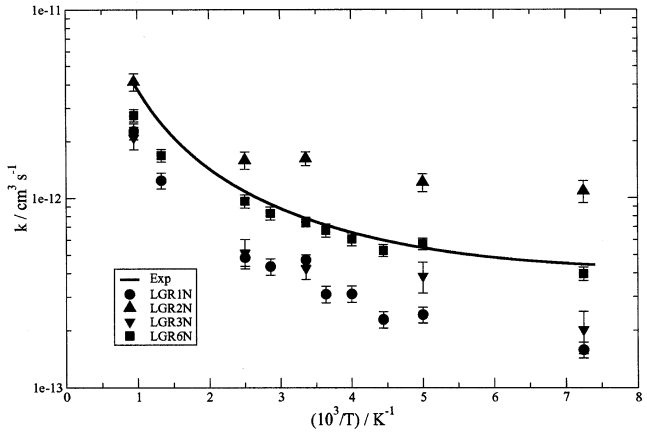

Figure 7. Rate coefficients plotted as a function of the inverse temperature: (solid line) recommended experimental results; (circles) LGR1N; (triangles up) LGR2N; (triangles down) LGR3N; (squares) LGR6N.

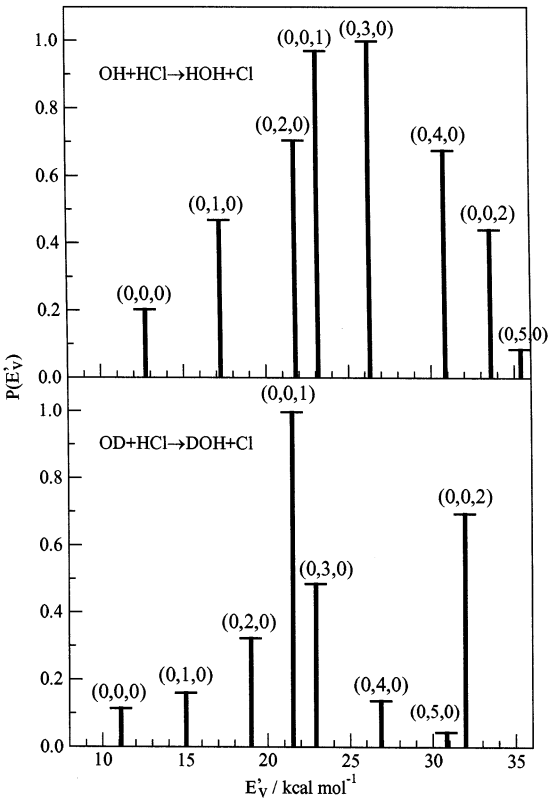

Figure 8. Vibrational distribution of the H_2O product (upper panel) and of the DOH product (lower panel) calculated on the LGR1N PES at $T = 298$ K. The labels (υ_{st1}, υ_{bend}, υ_{str2}) mean stretching of the old OH bond and bending and stretching of the new OH or OD bond, respectively. Only single bending and new OH or OD bond stretching excitations are shown.

frequencies at the saddle to reaction is also satisfactory (with the exception of the ω_3 frequency) and the imaginary frequency is exactly reproduced. As for the well (see Table 2), both structural and energetic data of the LGR1N well are close to the values obtained from the ab initio calculations[35] (deviations are smaller than 5%, except for the smallest frequencies).

We also generated three other PESs (LGR2N, LGR3N, and LGR4N) by playing with the height of the saddle to reaction and the depth of the van der Waals well. To this end, we varied p_o and d_o and adjusted the imaginary frequency of the system at the saddle to reaction. In LGR2N the height of the saddle to reaction was lowered to 1.00 kcal mol^{-1} while the depth of the well was kept at its ab initio value of −5.45 kcal mol^{-1}. In LGR3N the depth of the well was lowered to −6.50 kcal mol^{-1} and the height of the saddle to reaction was kept at 2.43 kcal mol^{-1}. Finally, in LGR4N the height of the saddle to reaction was lowered to 1.00 kcal mol^{-1} and the depth of the well was raised to −4.00 kcal mol^{-1}.

5.4. Dynamical Calculations. QCT rate coefficients, calculated on LGR1N by integrating batches of trajectories large enough to make the statistical error smaller than 10%, are small and systematically deviate from measured values by a factor of 2 (see Figure 7). Such a deviation from the measured values is larger than that for LGR3 (the percentual rms is 54%) definitely confirms the need for adjusting the ab initio features of the single electronically adiabatic surface. However, these results not only confirm that, as anticipated in ref 45, the new LAGROBO PES is sufficiently flexible to be moulded in a way that ensures the reproduction of the temperature dependence of the rate coefficients but also indicate that by playing in a concerted fashion with the saddle height and the well depth the experimental PVD can be reproduced. In fact, as already pointed out in the previous section, the entrance channel well plays a key role in enforcing a more appropriate allocation of the energy of the system into product vibration for both the OH + HCl and the OD + HCl reactions. The fraction of energy (the zero point energy has been always subtracted) disposed by LGR1N into products' vibration is 55% for both H_2O and DOH, well inside the interval 50−67% measured by the OD + HCl experiment.[42] Moreover, as shown in Figure 8 (for H_2O in the upper panel and DOH in the lower panel), the largest fraction of energy is disposed into the stretching mode for DOH and in the bending mode for H_2O, in agreement with the experimental findings. More quantitatively, the calculations give a fraction of 62% of the DOH product molecules excited in the OH stretching that well compares with a lower limit of 60 suggested by the experiment.

To better understand the role played by the height of the saddle and the depth of the well on the dynamical outcome, we extended the QCT calculations to the remaining LGR*x*N surfaces. On the LGR2N and LGR3N PESs QCT rate coefficients have been calculated in the range of 138−1055 K and are plotted in Figure 7. As apparent from the figure, the reactivity calculated on the LGR2N surface is significantly larger than the one calculated on the LGR1N PES, implying that a lowering of the height of the saddle to reaction from 2.43 to 1.00 kcal mol^{-1} is quite efficient in promoting reactivity. On the contrary, the values of the quasiclassical rate coefficients calculated on the LGR3N surface indicate only a slight increase of the reactivity with respect to LGR1N one. This again implies that, in the investigated range of temperature, an increase of the depth of the well has a minor effect in enhancing the efficiency of reaction. On the LGR4N surface only the rate coefficient at $T = 298$ K has been calculated. The value obtained (12.7×10^{-13} cm^3 molecule^{-1} mol^{-1}) is significantly higher

than the one obtained on the LGR1N surface (4.7×10^{-13} cm^3 molecule^{-1} mol^{-1}) though it is still slightly lower than the one obtained on the LGR2N surface (16.2×10^{-13} cm^3 molecule^{-1} mol^{-1}).

These results seem to confirm that there is a significant increase of the reactivity when the saddle to reaction is lowered whereas the effect is limited when the well depth is changed. As a consequence, further tests were mainly based on the modification of the height of the saddle to reaction (by leaving unchanged the depth of the van der Waals well as its ab initio value).

5.5. Need for a Finer Tuning. To further tune the structure of the LGR*x*N PESs to better reproduce the experiment, two new surfaces (LGR5N and LGR6N) were generated. In the case of LGR5N the energy of the saddle to reaction was set at 1.40 kcal mol^{-1} with no significant change for the geometries and the frequencies of the saddle to reaction and of the van der Waals complex. This change had a marked effect on the value of the rate coefficient calculated at $T = 298$ K (10.9×10^{-13} cm^3 molecule^{-1} mol^{-1}) that significantly exceeds the corresponding experimental value. In the case of LGR6N, as anticipated in ref 45, the energy of the saddle to reaction was set at 1.80 kcal mol^{-1} (the properties of both the saddle to reaction and the well of this surface are shown in Tables 1 and 2, with minor differences with the previous LAGROBO PESs). The agreement between the rate coefficient calculated at $T = 298$ K ($(7.5 \pm 0.4) \times 10^{-13}$ cm^3 molecule^{-1} mol^{-1}) and the experimental data motivated an increase of the number of trajectories integrated (the statistical error is now smaller than the 8%) and an extension of the quasiclassical calculations to the overall range of temperatures of the experiment. The calculated values of the rate coefficients are plotted in Figure 7. The plots evidence an improvement over the previous results (the percentual root-mean-square deviation is now 16%) even if the calculated values at higher temperatures underestimate the experimental ones. This means that LGR6N is the most accurate surface among the ones we have produced so far. At the same time, the product vibrational distributions calculated on LGR6N (see Figure 9) are also in line with the rationalization of the experiment of ref 42. In fact, whereas for the OD + HCl → DOH + H reaction the stretching of the new bond continues to be the most important (63% of the DOH molecules are formed with respect to the experimental lower limit of 60%), for the OH + HCl → H_2O + H reaction the vibrational excitation significantly populates the first three excited bending modes.

A last proof of the suitability of the LGR6N PES to describe the OH + HCl interaction comes from the calculation of the secondary kinetic isotopic effect, i.e., the ratio between the OD + HCl and OH + HCl rate coefficients. In fact, the value of the secondary kinetic isotopic effect calculated on the LGR6N PES at $T = 298$ K is 0.97 ± 0.11, in excellent agreement with the experimental value 1.01 ± 0.13.[34]

6. Conclusions

In this paper a "general purpose" procedure aimed at constructing functional representation of the interaction for four-atom systems has been illustrated. As a case study the OH + HCl reaction has been considered. By building on the success of a previous surface (LGR3) in reproducing the measured thermal rate coefficients and on the insuccess of the same surface in reproducing the measured isotopic effect in product vibrational distributions, we have further refined the fitting method and improved the multiproperty analysis of the OH + HCl

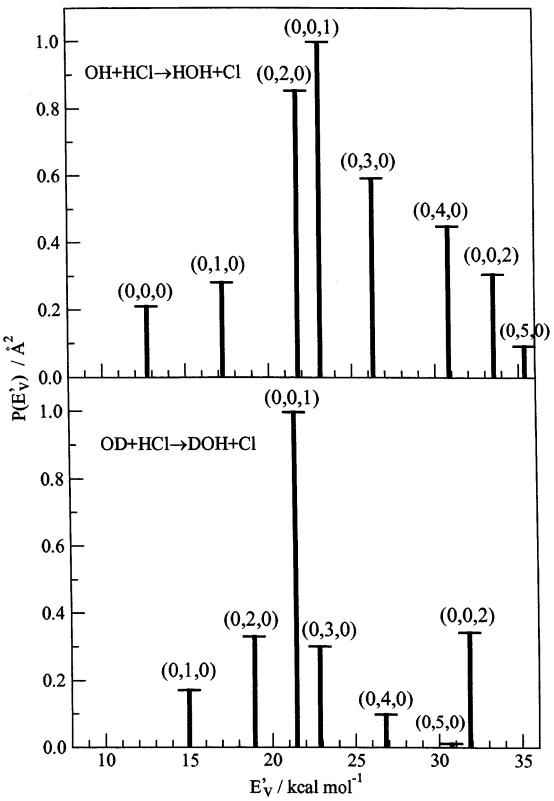

Figure 9. Vibrational distribution of the H_2O product (upper panel) and of the DOH product (lower panel) calculated on the LGR6N PES at $T = 298$ K. The labels (υ_{st1}, υ_{bend}, υ_{str2}) mean stretching of the old OH bond, and bending and stretching of the new OH or OD bond, respectively. Only single bending and new OH or OD bond stretching excitations are shown.

reaction. First, we incorporated into the LAGROBO functional the possibility of reproducing structured MEPs showing both minima and maxima. Second, we improved the generalizability of the surface adopting a new set of angular coordinates leading to a smooth behavior of the LAGROBO functional also at the edges of the interval of definition. Third, we simplified the use of the LAGROBO functional by establishing a more direct link between some of its parameters and the barrier height and the well depth. Fourth, we showed that it is possible to modify selectively the critical features of the PES (by playing with a few parameters) to significantly reduce the percentual root-mean-square deviation.

The best interpolated potential energy surface built using the improved LAGROBO functional for the OH + HCl reaction leads to results whose deviation from the experimental data are comparable with the error associated with both the statistics and the intrinsic limitations of quasiclassical treatments. This means that we reached a point in which it is appropriate to move a step forward by undertaking a fine-tuning process of the PES based on exact quantum dynamical calculations. This step, however, still presents large difficulties because exact full-dimensional four-atom quantum reactive studies (converged with total angular momentum) cannot (yet) be routinely performed on a single, albeit parallel, computer. Progress in this direction is, however, being made by implementing on the grid platform of a European Metalaboratory (a virtual laboratory made by several laboratories connected on a distributed computing platformystem) a simulator of crossed molecular beam experiments (SIMBEX)[46] that can efficiently deal also with exact quantum calculations.

Acknowledgment. Partial financial support from the MCyT, MIUR, ASI, and CNR is acknowledged. This work has been carried out as a part of the activity carried out in the D9 and D23 Actions of the COST in Chemistry European Initiative.

References and Notes

(1) Baer, M.; Kouri, D. J. In *Theory of Chemical Reaction Dynamics*; Clary, D. C., Ed.; Reidel: Dordrecht, The Netherlands, 1986; p 167.
(2) Bowman, J. M.; Schatz, G. C. *Annu. Rev. Phys. Chem.* **1995**, *46*, 169.
(3) *Modern Methods in Multidimensional Dynamics Computations in Chemistry*; Thompson, D. L., Ed.; World Scientific: Singapore, 1998.
(4) Hoffman, D. K.; Kouri, D. J. *Lecture Notes Chem.* **2000**, *75*, 57.
(5) Schatz, G. C. *Lecture Notes Chem.* **2000**, *75*, 15.
(6) Carter, S.; Handy, C. *Mol. Phys.* **1982**, *47*, 1445.
(7) Carter, S.; Handy, C. *Mol. Phys.* **1986**, *57*, 175.
(8) Lara, M.; Aguado, A.; Paniagua, M.; Roncero, O. *J. Chem. Phys.* **2000**, *113*, 1781.
(9) Laganà, A.; Crocchianti, S.; Faginas Lago, N.; Pacifici, L.; Ferraro, G. *Collect. Czech. Chem. Commun.* **2003**, *68*, xx.
(10) Laganà, A. *A* Molecular Dynamics Metalaboratory in Theory of the Dynamics of Elementary Chemical Reactions; NATO ARW Workshop, Balatonfoldvar, 2003.
(11) Garcia, E.; Laganà, A. *Mol. Phys.* **1985**, *56*, 621.
(12) Garcia, E.; Laganà, A. *Mol. Phys.* **1985**, *56*, 629.
(13) Paniagua, M.; Sanz, J. C.; Alvariño, J. M.; Laganà, A. *Chem. Phys. Lett.* **1986**, *126*, 330.
(14) Palmieri, P.; Garcia, E.; Laganà, A. *J. Chem. Phys.* **1988**, *88*, 181.
(15) Alvariño, J. M.; Laganà, A. *Chem. Phys. Lett.* **1990**, *168*, 449.
(16) Laganà, A.; Dini, M.; Garcia, E.; Alvariño, J. M.; Paniagua, M. *J. Phys. Chem.* **1991**, *95*, 8379.
(17) Laganà, A.; Alvariño, J. M.; Hernandez, M. L.; Palmieri, P.; Martinez, T.; Garcia, E *J. Chem. Phys.* **1997**, *106*, 10222.
(18) Parker, G. A.; Laganà, A.; Crocchianti, S.; Pack, R. T. *J. Chem. Phys.* Molecular Dynamics Metalaboratory in Theory of the Dynamics of Elementary Chemical Reactions**1995**, *102*, 1238.
(19) Huber, K. P.; Herzberg, G. *Molecular Spectra and Molecular Structure. IV. Constants of Diatomic Molecules*; Van Nostrand Reinhold: New York, 1979.
(20) Murrell, J. N.; Carter, S.; Farantos, S. C.; Huxley, P.; Varandas, A. J. C. *Molecular Energy Functionals*; Wiley: New York, 1984.
(21) Wilson, E. B.; Decius, J. C.; Cross, P. C. *Molecular Vibrations*; McGraw-Hill: New York, 1955.
(22) Laganà, A. *J. Chem. Phys.* **1991**, *95*, 2216.
(23) Garcia, E.; Laganà, A. *J. Chem. Phys.* **1995**, *103*, 5410.
(24) Laganà, A.; Ochoa de Aspuru, G.; Garcia, E. *J. Chem. Phys.* **1998**, *108*, 3886.
(25) Ochoa de Aspuru, G.; Clary, D. C. *J. Phys. Chem. A* **1998**, *102*, 9631. In this reference there is a misprint in the domain of existence of the δ angle that should read $-\pi/2 \leq \delta \leq \pi/2$.
(26) Pogrebnya, S. K.; Palma, J.; Clary, D. C.; Echave, J. *Phys. Chem. Chem. Phys.* **2000**, *2*, 693.
(27) Rodriguez, A.; Garcia, E.; Ceballos, A.; Laganà, A. *Chem. Phys. Lett.* **2001**, *333*, 471.
(28) Rodriguez, A.; Garcia, E.; Alvariño, J. M.; A. Laganà, *Chem. Phys. Lett.* **2001**, *345*, 219.
(29) Rodriguez, A.; Garcia, E.; Hernandez, M. L.; Laganà, A. *Chem. Phys. Lett.* **2002**, *360*, 304.
(30) Clary, D. C.; Nyman, G.; Hernandez, R. *J. Chem. Phys.* **1994**, *101*, 3704.
(31) Murrell, J. N.; Carter, S. *J. Phys. Chem.* **1917**, *21*, 4887.
(32) Clary, D. C. *J. Chem. Phys.* **1991**, *95*, 7298.
(33) Steckler, R.; Thurman, G. M.; Watts, J. D.; Bartlett, R. J. *J. Chem. Phys.* **1997**, *106*, 3926.
(34) Battin-Leclerc, F.; Kim, I. K.; Talukdar, R. K.; Portmann, R. W.; Ravishankara, A. R.; Steckler, R.; Brown, D. *J. Phys. Chem. A* **1999**, *103*, 3227.
(35) Yu, H.-G.; Nyman, G. *J. Chem. Phys.* **2000**, *113*, 8936.
(36) Molina, M. J.; Molina, L. T.; Smith, C. A. *Int. J. Chem. Kinet.* **1984**, *16*, 1151.
(37) Keyser, L. F. *J. Phys. Chem.* **1984**, *88*, 4750.
(38) Husain, D.; Plane, J. M. C.; Xiang, C. C. *J. Chem. Soc., Faraday Trans. 2* **1984**, *80*, 713.
(39) Ravishankara, A. R.; Wine, P.; Wells, J. R.; Thompson, R. L. *Int. J. Chem. Kinet.* **1985**, *17*, 1281.
(40) Sharkey, P.; Smith, I. W. M. *J. Chem. Soc., Faraday Trans. 2* **1993**, *89*, 631.
(41) Atkinson, R.; Baulch, D. L.; Cox, R. A.; Hampson, R. F., Jr.; Kerr, J. A.; Rossi, M. J.; Troe, J. *J. Phys. Chem. Ref. Data* **2000**, *29*, 167.
(42) Butkovskaya, N. I.; Setser, D. W.; *J. Chem. Phys.* **1998**, *108*, 2434.
(43) Herzberg, G. *Molecular Spectra and Molecular Structure. II. Infrared and Raman Spectra of Polyatomic Molecules*; Van Nostrand Reinhold: New York, 1945.
(44) Steckler, R.; Hu, W.-P.; Liu, Y.-P.; Lynch, G. C.; Garrett, B. C.; Isaacson, A. D.; Lu, D.-H.; Melissas, V. S.; Truong, T. N.; Rai, S. N.; Hancock, G. C.; Lauderdale, J. G.; Joseph, T.; Truhlar, D. G. *QCPE Bull.* **1995**, *15*, 32.
(45) Rodriguez, A.; Garcia, E.; Hernandez, M. L.; Laganà, A. *Chem. Phys. Lett.* **2003**, *371*, 223.
(46) Gervasi, O.; Laganà, A.; Lobbiani, M. *Lecture Notes Comput. Sci.* **2002**, *2331*, 956.